Utilizing SrSi₂O₂N₂:Eu²⁺,Yb²⁺ phosphor to achieve high hue rendering index and high hue stability

Ha Thanh Tung[1], **Dieu An Nguyen Thi[2]**

[1]Faculty of Basic Sciences, Vinh Long University of Technology Education, Vinh Long Province, Vietnam
[2]Faculty of Electrical Engineering Technology, Industrial University of Ho Chi Minh City, Ho Chi Minh City, Vietnam

Article Info	ABSTRACT
	For white-light emitting diode (WLED) applications, a green-to-orange emission nitridosilicate-based phosphor is created. The observed wide-band radiation in the green-orange range is caused by Eu^{2+} and Yb^{2+} at the trap point of a doubly doped $SrSi_2O_2N_2$:Eu^{2+},Yb^{2+} (SSON:Eu,Yb) nitridosilicate phosphor. The green-color radiation's decay duration was measured to validate the energy transfer among activator ions. The co-doping various ratios' influence of activator ions on luminescence features was investigated. The resulting phosphor's radiation is a function of the activator ion concentrations and raising the Yb^{2+} concentration causes red-color radiation to dominate the green radiation. To generate white illumination, the resulting phosphor was coupled with an InGaN blue-LED chip having a pumping wavelength of 450 nm. Two stages were taken to achieve hue balance management. Initially, the green to orange proportion was tuned by varying the Eu^{2+} and Yb^{2+} ions' concentrations. At the second stage, the Commission Internationale de L'Eclairage, International Commission on Illumination (CIE) coordinates were changed from [0.2805; 0.2014] to [0.4071; 03789] by raising the amount of phosphor powder used. White illumination produced under optimal conditions has a hue rendering indicator of 89. The designed single-stage dual-hue-releasing nitridosilicate phosphor and blue-LED chip displayed remarkable hue steadiness over a wideband of forward-bias currents (100 to 500 mA at 3 V).

Corresponding Author:

Dieu An Nguyen Thi
Faculty of Electrical Engineering Technology, Industrial University of Ho Chi Minh City
No. 12 Nguyen Van Bao Street, Ho Chi Minh City, Vietnam
Email: nguyenthidieuan@iuh.edu.vn

1. INTRODUCTION

Nowadays, InGaN-based diodes emit white-light emitting diode (WLED) are gaining popularity in the future illumination stage owing to the numerous benefits when they are utilized in incandescent bulbs, including high performance, an ecologically friendly character, dependability, small size, longevity, and so on [1], [2]. The most typical method to generate white illumination is to mix an InGaN blue LED chip with a $Y_3Al_5O_{12}$:Ce^{3+} (YAG) yellow phosphor [3]. Nevertheless, the use of them is restricted since the emitted illumination cannot achieve a good color balance for accurate color representation without the presence of red illumination. To address this issue, several phosphor-based LEDs were used to boost red luminescence [4]. The multiple-phosphor technique outperforms the YAG:Ce^{3+} blue LED chip technique in terms of color rendering (Ra), effectiveness, and luminosity. Nonetheless, the varying heat quenching of the separate phosphors produces color rendering aberration versus supplied power, as well as an improvement in productivity expense for actual usage. The varied phases of phosphors, on the other side, cause a decrease in

illuminating effectiveness according to the re-absorptivity within multi-phosphor-based LEDs [5], [6]. The use of a filled-hue producing one-phase phosphor built by oxide and silicate compositions led to a highly steady color rendering against a supplied power [7]–[9].

Lately, nitridosilicate and oxynitridosilicate-based down-transformation phosphors have demonstrated excellent temperature stability and good illuminating performance [10], [11]. Hedili *et al.* [10] noted the illuminating characteristics and configuration of a Eu^{2+} and Yb^{2+} doped $SrSi_2O_2N_2$ (SSON) oxynitridosilicate phosphor with wide-range emission in the green to orange area, a full width at half maximum (FWHM) (entire breadth at half-maximal) of 170 nm, and exterior quantum productivity of about 16% with 450 nm stimulation [12]–[14]. The transferring power from Eu^{2+} and Yb^{2+} ions was validated by the writers. The configuration among luminescence characteristics of a two-hue producing $SSON:xEu^{2+}$, yYb^{2+} oxynitridosilicate are described in this study. The resulting phosphor was employed as a solitary illumination converter link to a blue-releasing LED chip to provide heated illumination which has a great hue rendering indicator and steady Commission Internationale de L'Eclairage, International Commission on Illumination (CIE) over a broad forward-bias current range.

2. EXPERIMENTAL

SSON:Eu,Yb green to orange illuminating phosphor was synthesized using Si_3N_4, $SrCO_3$, Eu_2O_3, and Yb_2O_3. All components with a purity of at least 3N were utilized with no additional cleanse. The stoichiometric number of the initial components was carefully combined with ethanol and mixed in an agate mortar before going through 2-hour drying in an oven at 120 °C. We packed the powder mixes in an alumina crucible and heated them in a horizontal alumina tube furnace with a N_2/H_2 (5%) gas flow, at 1400 °C, lasting 8 hours. The doses of Eu^{2+} ion stayed at 2 at% in comparison to Sr^{2+} ion, whereas the Yb^{2+} ion quantity was changed 0% to 8%. After burning, a gently sintered specimen was acquired, which was subsequently preliminary turned into fine powders by grinding. These fine powders were then used to produce white-light LED. The resulting SSON:Eu,Yb powder was integrated with silicon resin. After that, we packed them above an InGaN-based blue chip and left them dry at 120 °C for 2 hours [15], [16].

Analyses of phase composition were performed using an X-ray diffractometer; with Cu Kα (λ=1.542 Å) at normal temperature. We also examined the microstructure of the produced powder using the scanning electron microscope. At normal temperature, the luminescence spectra were achieved utilizing a fluorescence spectrophotometer with a 150 W Xe light as a stimulation supply. The decomposition period was measured using the streak camera C4334. The integrated sphere approach was used to calculate quantum effectiveness. PTE-VUVD2L-100 was used to evaluate heat quenching.

3. RESULTS AND DISCUSSION

As maximum points of all specimens' X-ray diffraction patterns are reasonably close to the SSON reference. In comparison to the findings provided by Chen *et al.* [15], the produced outcome includes almost entirely a solitary stage. It also has no substantial amounts of impurities like Sr_2SiO_4. When there is the addition of Yb^{2+}, a high point at 28°, this may be seen in numerous specimens, although its origin is unknown. Eu^{2+} (1.17 Å, 6-coordination number) and Yb^{2+} (1.14 Å, octahedral coordination) have ionic radii that are similar to Sr^{2+} (1.18 Å, 6-CN.) As previously demonstrated, Eu^{2+}-Yb^{2+} cations preferentially inhabit the Sr^{2+}-points within the SSON lattice. The solid-solution phase formation when SSON is doped with Eu^{2+}-Yb^{2+} is suggested by the minor displacement of the position of the X-Ray diffraction analysis (XRD) peaks in our studies [17]–[19].

The $SSON:Eu^{2+}$ phosphor emitting spectra reveal a solitary emitting range reached a peak at 540 nm, which is ascribed toward the Eu^{2+} ion's $4f^65d^1 \rightarrow 4f^75d^0$ transfer. Based on the increased degree of covalency among the activator ion and surrounded ligands, the radiation is noticed at longer wavelengths when tried to compare to common silicate/aluminate-based phosphors. The emitting band has a FWHM of 76 nm. The stimulation bands of color of Eu^{2+} at 540 nm indicate a stimulation range within the region 200 to 500 nm. The stimulation spectra contain multiple unresolved sub-bands attributable to Eu^{2+} ion stimulated states $4f^65d^1$. The radiation of Yb^{2+} doped SSON phosphor is a solitary radiation range that peaks at 612 nm and is ascribed to relaxation to the $4f^{13}5d^0$ stage of Yb^{2+} ions (FWHM=130 nm). The stimulation $SSON:Yb^{2+}$ phosphors' bands of color are composed of many ranges, one of which is attributed to the f−d transfer. The light was attributed to Yb^{2+}-trapped exciton luminescence. Notably, the stimulation spectra of $SSON:Yb^{2+}$ are overlapped by part with the emitting spectrum of $SSON:Eu^{2+}$ phosphor within the 470 to 550 nm region. The power transferring ratio is proportional to the spectral overlapping among the emitting range of the power donor (Eu^{2+}) and the absorption range of the power acceptor (Yb^{2+}).

The light decomposition curves could be greatly represented by dual-exponential decomposition curve in (1) [20]:

$$I = I_0 + A_1 e^{-\frac{t}{\tau_1}} + A_2 e^{-\frac{t}{\tau_2}} \qquad\qquad (1)$$

Here, I is the luminous strength; t denotes the duration; A_1 and A_2 are constant factors; τ_1 and τ_2 denote the short and long lifespan for exponential elements, in turn. The mean decay period ($\tau *$) can be computed using (2) according to the specified numbers for all of the parameters as stated before [21]:

$$\tau *= (A_1{\tau_1}^2 + A_2{\tau_2}^2)/(A_1\tau_1 + A_2\tau_2) \qquad\qquad (2)$$

Once the converting phosphor is in near closeness to the LED chip, its heating behavior is critical. Because of the little chip surface and restricted phosphor region, heating control is a significant consideration in LED configuration. Heats of 400 to 450 K can be attained close to the LED chip, though. Consequently, even at these high temperatures, the phosphor must retain quantum effectiveness and spectrum properties. The former is determined by the total emission strength being thermally quenched. In the latter case, changing and/or expanding the emission spectrum can change the overall emitting color of the device. Furthermore, the stimulation spectrum can shift, impacting the imbibed tiny part of the pumping LED's output. As a result, a phosphor assessment needs to include a minimum of research on heat extinguishing behavior, which means the change of emitting strength (preferably the quantum effectiveness). The decay period of luminescence in first order has comparable temperature behavior to that of strength quenching.

Figure 1 illustrates the opposite shift between the SSON:Eu,Yb and YAG:Ce^{3+} weight percentages for retaining mean correlated color temperatures (CCTs). Additionally, this inverse proportion contributes to influencing the dispersion and absorbance of light beams in WLED's double-film configuration, which greatly impacts the WLEDs' color standard and illuminating effectiveness. Thus, the SSON:Eu,Yb concentration chosen specifies the WLEDs hue standard. Once the SSON:Eu,Yb proportion raised 2% to 20% wt., the YAG:Ce^{3+} dosage declined to retain the median CCTs. WLEDs with hue temperatures among 5600 K and 8500 K also exhibit this characteristic.

Figure 2 shows SSON:Eu,Yb green phosphorus concentration has an influence on the WLEDs' transmission spectrum at 3000 K CCT. It is feasible to choose depending on the requirements provided by the producer [22]. WLEDs that need high hue quality might somewhat reduce illumination. Figure 2 shows white illumination is the combination of the spectral area. As can be seen, the strength trend rises with SSON:Eu,Yb content in 420 to 480 nm and 500 to 640 nm emission wavelengths. The shift in the two-range emitting bands of hue indicates the growth in illumination generating intensity. Furthermore, the enhancement in blue-illumination dispersion in WLEDs implies that the dispersion of light within the phosphor package of the WLED is improved and helps to achieve better chromatic consistency and fidelity. It is well-known that managing to achieve better color uniformity with CCT greater than 5000 K is challenging for remote-phosphor configuration. These results, however, proved that SSON:Eu,Yb could help the producers to reach their goal of regulating color quality at poor and elevated CCTs (5600 K and 8500 K).
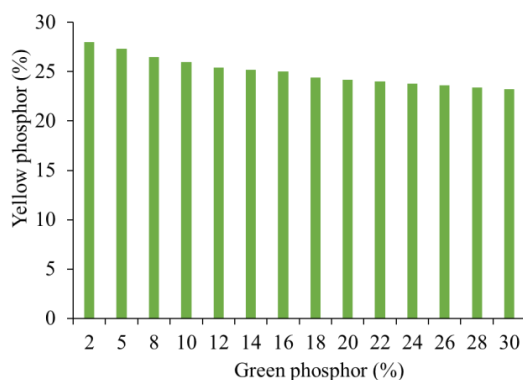

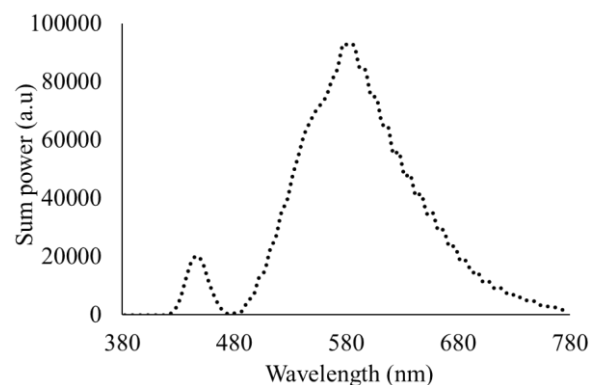Figure 1. Adjusting the dosage of phosphor to maintain the median CCT

Figure 2. The emitting bands of hue of 3000 K WLEDs as a function of SSON:Eu,Yb dosage

Figure 3 illustrates the luminous flux emitted rises dramatically when the SSON:Eu,Yb concentration raised 2% wt. to 20% wt. This confirmed the effectiveness SSON:Eu,Yb remote layer in

improving WLED luminous strength. Next, the color divergence was investigated and demonstrated in Figure 4. The figure showed that the variation in chromaticity notably declined with the phosphor SSON:Eu,Yb proportion in all median CCTs. This can be explained by the absorbance feature of the SSON:Eu,Yb green phosphor. When the SSON:Eu,Yb phosphor collects the LED-chip blue illumination, it generates green radiation from converting the absorbed blue one. SSON:Eu,Yb also collect YAG:Ce-emitted yellow rays but owing to the absorbing qualities of the material, the blue-illumination absorption is greater. Hence, the addition of SSON:Eu,Yb encourages the green-emission parts in WLEDs to grow, leading to a more homogeneous chromaticity. Uniformity of chromaticity is a crucial feature among the latest parameters of the modern WLED lamp. Thus, possessing a high color-uniformity specification could contribute to increasing the price of a WLED lamp in the marketplace. The advantage of employing SSON:Eu,Yb is its inexpensive cost. SSON:Eu,Yb can thus be commonly employed.

Hue homogeneity is only one factor to look at in the assessment of WLEDs' chromaticity performance. Hue quality cannot be claimed to be good when it only has a good indicator of color uniformity. Thus, another parameter was developed to combine the color uniformity with other evaluation factors This indicator is color quality scale (CQS), which can access the color rendition indicator (CRI) and color uniformity while considering the visual inclination of observers [23]–[25]. The data recorded on CQS is shown in Figure 5, in which the growth in CQS in the existence of the distant phosphor film SSON:Eu,Yb is observed. Additionally, the CQS does not significantly change with SSON:Eu,Yb concentrations lower than 10% wt., when the SSON:Eu,Yb concentration is increased. Besides, this study demonstrates the CRI results to observe the influence of SSON:Eu,Yb on each color indicator. The CRI results depicted in Figure 6 show that the phosphor SSON:Eu,Yb is not advantageous for this indicator. CRI shows a small reduction when there is the distant phosphor SSON:Eu,Yb sheet. Additionally, when the SSON:Eu,Yb concentration exceeds 10% wt., CQS and CRI decrease remarkably based on severe hue loss when green emission is so intense that breaks the color balance of the chroma range (including blue, green, and yellow) [26], [27]. Consequently, we should choose the suitable concentration of SSON:Eu,Yb to meet the specific lighting requirements.
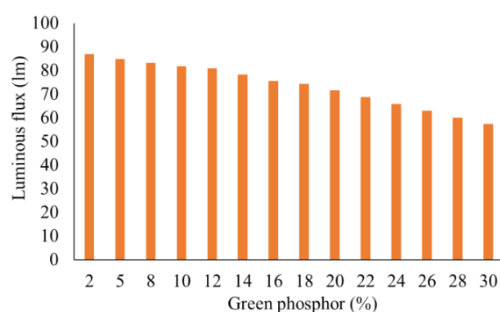

Figure 3. The luminous flux of WLEDs as a function of SSON:Eu,Yb dosage
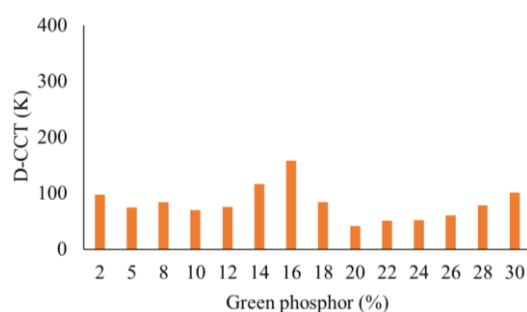

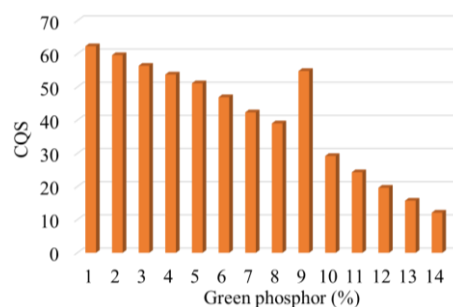Figure 4. The hue deviation of WLEDs as a function of SSON:Eu,Yb dosage

Figure 5. The hue quality scale of WLEDs as a function of SSON:Eu,Yb dosage
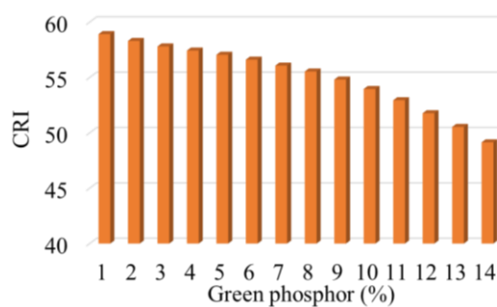

Figure 6. The hue rendering index of WLEDs as a function of SSON:Eu,Yb dosage

The assessment would be carried out through a greater series containing fifteen distinctive hue patterns that exhibit greater saturation compared to the eight patterns mentioned earlier. R_a would be assessed via the hue disparity for the eight patterns, indicating that the significant hue disparity of a single

pattern merely slightly diminishes CRI. For CQS assessment, the root mean square aberration would be employed, negatively affecting huge disparities in a greater way. CRI carries a downside in that minimal value zero of R_a does not exist. In one instance, assessment results in one R_a value of -47 in the case of small pressure sodium lights. CQS can solve the downside by employing a normalization formula, giving various results in the range of 0 to 100 [26]:

$$R_{new} = 10 \cdot ln[exp(R_{old}/10) + 1] \tag{3}$$

Human usually perceive items through clear and saturated hues instead of rays giving flat looks. Such a behavior resulted in creating elements to assess the attractiveness of items lit by testing ray. Compared to sun ray, particular rays can give items a better appearance, resulting in a CRI over 100. All hue disparities among the testing ray and the reference ray would result in an R_a falling under 100, since the reference ray would be identical to a "sublime" ray. Judging CQS' nature, rays resulting in hue generation items having identical hue and greater saturation compared to the reference ray, receive no penalty, save for the "sublime" CQS value. For CRI, rays that exhibit huge (blue) as well as small (red) CCT may still give one huge R_a result, which applies to reference rays with identical CCTs. On the other hand, the hue generation capability for these rays would be small. The rays merely generate lesser hue scale uncanny to human eyes. CQS applies lesser rendering index to such rays, based on the hue scale zone for fifteen hue patterns. CQS holds many advantages to surpass CRI. On the other hand, this element is affected by the task of choosing reference rays or unlimited quantity for reference rays for our study, since the reference rays is determined by the testing ray's CCT.

4. CONCLUSION

Finally, for the first time, a two-hue releasing SSON:Eu,Yb oxynitridosilicate phosphor for solitary usage in a heated white LED has been produced. The SSON:Eu,Yb phosphor produced exhibits wide range emitting concentrated at 540 and 612 nm for the Eu^{2+} and Yb^{2+} ions, accordingly. The proportionate percentage of green and orange radiations was revealed for being dependent upon this activator ion concentration of the phosphor. The power transmission from Eu^{2+} ion to Yb^{2+} trapping sites was verified by the rapid decay period of Eu^{2+} radiation. The white LED, which combines a 450 nm producing InGaN chip with a dual-hue producing SSON:Eu,Yb phosphor, emits heated white illumination with a great hue rendering indicator and outstanding hue steadiness versus energy supply.

REFERENCES

[1]   A. Hassan, S. Khan, K. Rasul, and A. Hussain, "Lensless on-chip LED array microscope using amplitude and phase masks," *Journal of the Optical Society of America B*, vol. 37, no. 12, p. 3652, Dec. 2020, doi: 10.1364/JOSAB.396076.

[2]   X. Gao *et al.*, "Circularly polarized light emission from a GaN micro-LED integrated with functional metasurfaces for 3D display," *Optics Letters*, vol. 46, no. 11, p. 2666, Jun. 2021, doi: 10.1364/OL.415150.

[3]   S. Zhang *et al.*, "Efficient emission of InGaN-based light-emitting diodes: toward orange and red," *Photonics Research*, vol. 8, no. 11, p. 1671, Nov. 2020, doi: 10.1364/PRJ.402555.

[4]   T. Zhang, X. Zhang, B. Ding, J. Shen, Y. Hu, and H. Gu, "Homo-epitaxial secondary growth of ZnO nanowire arrays for a UV-free warm white light-emitting diode application," *Applied Optics*, vol. 59, no. 8, p. 2498, Mar. 2020, doi: 10.1364/AO.385656.

[5]   H. Goo, S. Mo, H. J. Park, M. Y. Lee, and J.-C. Ahn, "Treatment with LEDs at a wavelength of 642 nm enhances skin tumor proliferation in a mouse model," *Biomedical Optics Express*, vol. 12, no. 9, p. 5583, Sep. 2021, doi: 10.1364/BOE.427205.

[6]   M. V. -Treviño, J. G. -Gutiérrez, J. M. R. -Lelis, and E. L. Apreza, "Optimizing an LED array for an infrared illumination source using the near field for venous pattern detection," *Applied Optics*, vol. 59, no. 9, p. 2858, Mar. 2020, doi: 10.1364/AO.381815.

[7]   V.-C. Su and C.-C. Gao, "Remote GaN metalens applied to white light-emitting diodes," *Optics Express*, vol. 28, no. 26, p. 38883, Dec. 2020, doi: 10.1364/OE.411525.

[8]   A. D. Griffiths *et al.*, "Multispectral time-of-flight imaging using light-emitting diodes," *Optics Express*, vol. 27, no. 24, p. 35485, Nov. 2019, doi: 10.1364/OE.27.035485.

[9]   Z.-H. Xu, W. Chen, J. Penuelas, M. Padgett, and M.-J. Sun, "1000 fps computational ghost imaging using LED-based structured illumination," *Optics Express*, vol. 26, no. 3, p. 2427, Feb. 2018, doi: 10.1364/OE.26.002427.

[10]   M. K. Hedili, B. Soner, E. Ulusoy, and H. Urey, "Light-efficient augmented reality display with steerable eyebox," *Optics Express*, vol. 27, no. 9, p. 12572, Apr. 2019, doi: 10.1364/OE.27.012572.

[11]   E. M. A. Anas, H. K. Zhang, J. Kang, and E. Boctor, "Enabling fast and high quality LED photoacoustic imaging: a recurrent neural networks based approach," *Biomedical Optics Express*, vol. 9, no. 8, p. 3852, Aug. 2018, doi: 10.1364/BOE.9.003852.

[12]   M. A. Khan, R. Takeda, Y. Yamada, N. Maeda, M. Jo, and H. Hirayama, "Beyond 53% internal quantum efficiency in a AlGaN quantum well at 326 nm UVA emission and single-peak operation of UVA LED," *Optics Letters*, vol. 45, no. 2, p. 495, Jan. 2020, doi: 10.1364/OL.376894.

[13]   H. Gu, M. Chen, Q. Wang, and Q. Tan, "Design of two-dimensional diffractive optical elements for beam shaping of multicolor light-emitting diodes," *Applied Optics*, vol. 57, no. 10, p. 2653, Apr. 2018, doi: 10.1364/AO.57.002653.

[14]   E.-L. Hsiang, Q. Yang, Z. He, J. Zou, and S.-T. Wu, "Halo effect in high-dynamic-range mini-LED backlit LCDs," *Optics Express*, vol. 28, no. 24, p. 36822, Nov. 2020, doi: 10.1364/OE.413133.

[15]   D. Chen *et al.*, "Improved electro-optical and photoelectric performance of GaN-based micro-LEDs with an atomic layer

deposited AlN passivation layer," *Optics Express*, vol. 29, no. 22, p. 36559, Oct. 2021, doi: 10.1364/OE.439596.

[16] W. Wang and P. Zhu, "Red photoluminescent Eu 3+ -doped Y 2 O 3 nanospheres for LED-phosphor applications: Synthesis and characterization," *Optics Express*, vol. 26, no. 26, p. 34820, Dec. 2018, doi: 10.1364/OE.26.034820.

[17] K. Chung, J. Sui, T. Sarwar, and P.-C. Ku, "Feasibility study of nanopillar LED array for color-tunable lighting and beyond," *Optics Express*, vol. 27, no. 26, p. 38229, Dec. 2019, doi: 10.1364/OE.382287.

[18] T. Kozacki, M. Chlipala, and P. L. Makowski, "Color Fourier orthoscopic holography with laser capture and an LED display," *Optics Express*, vol. 26, no. 9, p. 12144, Apr. 2018, doi: 10.1364/OE.26.012144.

[19] J. Li, F. Wang, M. Zhao, F. Jiang, and N. Chi, "Large-coverage underwater visible light communication system based on blue LED employing equal gain combining with integrated PIN array reception," *Applied Optics*, vol. 58, no. 2, p. 383, Jan. 2019, doi: 10.1364/AO.58.000383.

[20] A. Lihachev, E. V. Plorina, M. Lange, I. Lihacova, A. Derjabo, and D. Bliznuks, "Imaging of LED-excited autofluorescence photobleaching rates for skin diagnostics," in *Clinical and Preclinical Optical Diagnostics II*, J. Q. Brown and T. G. van Leeuwen, Eds., SPIE, Jul. 2019, p. 63. doi: 10.1117/12.2526260.

[21] H. Liu *et al.*, "TuLUMIS - a tunable LED-based underwater multispectral imaging system," *Optics Express*, vol. 26, no. 6, p. 7811, Mar. 2018, doi: 10.1364/OE.26.007811.

[22] R. H. Horng, S. Sinha, C. P. Lee, H. A. Feng, C. Y. Chung, and C. W. Tu, "Composite metal substrate for thin film AlGaInP LED applications," *Optics Express*, vol. 27, no. 8, p. A397, Apr. 2019, doi: 10.1364/OE.27.00A397.

[23] P. Manley, S. Walde, S. Hagedorn, M. Hammerschmidt, S. Burger, and C. Becker, "Nanopatterned sapphire substrates in deep-UV LEDs: is there an optical benefit?," *Optics Express*, vol. 28, no. 3, p. 3619, Feb. 2020, doi: 10.1364/OE.379438.

[24] X.-X. Xia *et al.*, "LED-based fiber quantum key distribution: toward low-cost applications," *Photonics Research*, vol. 7, no. 10, p. 1169, Oct. 2019, doi: 10.1364/PRJ.7.001169.

[25] Q.-H. Pham, J.-C. Chen, and H.-B. Nguyen, "Reducing Efficiency Droop in (In,Ga)N/GaN Light-emitting Diodes by Improving Current Spreading with Electron-blocking Layers of the Same Size as the n-pad," *Current Optics and Photonics*, vol. 4, no. 4, pp. 380–390, 2020, doi: 10.3807/COPP.2020.4.4.380.

[26] J. Yan *et al.*, "Uniting GaN Electronics and Photonics on A Single Chip," *Journal of Lightwave Technology*, vol. 39, no. 19, pp. 6269–6275, Oct. 2021, doi: 10.1109/JLT.2021.3094850.

[27] C. Zhao, C. W. Tang, B. Lai, G. Cheng, J. Wang, and K. M. Lau, "Low-efficiency-droop InGaN quantum dot light-emitting diodes operating in the 'green gap,'" *Photonics Research*, vol. 8, no. 5, p. 750, May 2020, doi: 10.1364/PRJ.380158.

BIOGRAPHIES OF AUTHORS

Ha Thanh Tung 🔟 [icons] received the PhD degree in Physics from University of Science, Vietnam National University Ho Chi Minh City, Viet Nam, he is working as a lecturer at the Faculty of Basic Sciences, Vinh Long University of Technology Education, Viet Nam. His research interests focus on developing the patterned substrate with micro and nano-scale to apply for physical and chemical devices such as solar cells, OLED, and photoanode. He can be contacted at email: tunght@vlute.edu.vn.

Dieu An Nguyen Thi 🔟 [icons] received a master of Electrical Engineering, HCMC University of Technology and Education, Viet Nam. Currently, she is a lecturer at the Faculty of Electrical Engineering Technology, Industrial University of Ho Chi Minh City, Vietnam. Her research interests are theoretical physics and mathematical physics. She can be contacted at email: nguyenthidieuan@iuh.edu.vn.